JOURNAL OF MATERIALS SCIENCE 25 (1990) 3439–3448

Spherical-impact damage and strength degradation in Si_3N_4–SiC composites

YOSHIO AKIMUNE
Scientific Research Laboratory, Central Engineering Laboratories, Nissan Motor Co. Ltd, 1 Natsushima-cho, Yokosuka 237, Japan

Four types of SiC-whisker/silicon nitride and SiC-particle/silicon nitride composites were produced, and their mechanical properties and impact damage behaviour examined. All of the composites exhibited elastic response behaviour at spherical impact with Hertz cone crack initiation. Impact resistance behaviour, however, was different for each composite. This was due to the different mechanical properties produced by their microstructures. A SiC-platelet/silicon nitride composite displayed the highest resistance to crack initiation and propagation, which resulted in high impact resistance to strength degradation. On the other hand, SiC-particle/silicon nitride, SiC-whisker/silicon nitride, and large SiC-whisker/silicon nitride composites showed less impact resistance, even though they have higher mechanical properties such as bending strength and fracture toughness.

1. Introduction

Silicon nitride is a candidate material for heat engine components because of its high bending strength, high heat resistance, and moderate fracture toughness values [1]. However, a demand exists, to increase the fracture toughness of silicon nitride even more to make it suitable for anticipated gas turbine component applications [2]. Many strengthening methods have been developed for this purpose, including the use of fibre and whisker reinforcement and particle dispersion for fibre pullout [3], crack deflection [4], crack bowing [5], and microcracking [6]. Through these studies the mechanical properties of silicon nitride [7–10] have been improved.

Reinforcement of silicon nitride by SiC-whisker or particle dispersion has been studied extensively [9, 10]. An improved process has been reported through which the fracture toughness and strength of Si_3N_4 composites has been improved. The mechanical properties of these composites, however, depend on the whisker shape and characteristics [11]. Further efforts to create microstructures that will produce high fracture toughness are underway. It is well known, however, that the whisker and particle shape and characteristics are also related to the sintering behaviour of silicon nitride and to the silicon nitride matrix itself [12]. As a result, SiC whisker and particle characteristics are believed to have an influence on the mechanical properties of ceramic composites [13, 14].

On the other hand, impact damage is a serious problem in turbine components [15–17]. Even when using Si_3N_4 composites, the possibility exists of damage occurring due to particle impact or point indentation. There have been a few recent reports on the practical use of composite ceramics for erosion resistance [18], contact damage [19], and impact damage [20]. Before silicon nitride composites can be given practical application as engine components, however, impact damage and erosion studies must be conducted in line with those studies already completed on impact damage and strength degradation [21–24].

The present study evaluates the mechanical properties and impact damage behaviour of hot-pressed SiC-particle/silicon nitride and SiC-whisker/silicon nitride composites made from different types of SiC particles and whiskers. Spherical impact damage to and strength degradation of these composites were examined at room temperature. The relationship between the mechanical properties of the composites and their respective microstructures (as influenced by the addition of different SiC particles and whiskers) was, therefore, studied using scanning electron microscopy (SEM) and transmission electron microscopy (TEM).

2. Experimental procedure

2.1. Materials

Commercially produced silicon nitride (Si_3N_4) powder, SiC-particles, SiC-platelets, and two types of SiC whiskers (10 vol %), were obtained (Table I). Each SiC additive was mixed together with Si_3N_4 powder in a ball mill together with 5 wt % yttria (5 wt % ytrria and 5 wt % alumina were pre-mixed in the UBE COA powder) using ethanol as the solvent. After ball-milling, the slurry was dried in a rotary evaporator and sieved to $< 210\,\mu m$. The Si_3N_4 and mixed SiC-whisker/Si_3N_4 powders were then hot-pressed at 30 MPa pressure under 0.1 MPa nitrogen in a BN-coated graphite mould for 0.5 h at 1700 and 1780° C, respectively. Four types of Si_3N_4–SiC composites and hot-pressed Si_3N_4 (HPSN) as a reference were obtained.

The 50 mm by 40 mm by 6 mm hot-pressed plates were ground to eliminate the surface graphite layer, and then they were cut into 4 mm by 3 mm by 40 mm specimens for mechanical testing. Impact testing

0022–2461/90 $03.00 + .12

specimens (6 mm by 3 mm by 50 mm) were polished using two grades of diamond paste (6 and 3 μm) to eliminate machine damage to the surface layer and produce mirror-like flat and parallel surfaces. A four-point bending test (inner span 10 mm, outer span 30 mm) with the crack plane parallel to the hot-press direction and at a cross-head speed of 0.5 mm min^{-1} was used to measure bending strength. The results were analysed using Weibull statistics [25]. Fracture toughness was measured by the indentation method [26], Young's modulus by resonance, and hardness by a Vickers indentor with a 300 g weight.

2.2. Impact test

In the impact test [20, 24], a partially stabilized zirconia (PSZ) sphere (1.0 mm diameter) was shot into a specimen in the hot-pressed direction by a helium gas pistol at room temperature. The PSZ sphere was attached to the top of a plastic sabot with a small magnet. The sabot was set in the pistol of the apparatus after the gas pressure from a helium gas cylinder had risen to a specified level in the chamber. The diaphragm was then punctured by a needle, releasing the gas towards the pistol. The sabot was driven towards the end of the steel pipe at a rate dependent on the amount of gas released. At the end of the pipe, the motion of the sabot was abruptly stopped, ejecting the sphere towards the target. The direction of the sphere is parallel to the hot-pressing direction.

The velocity of sabot, including the PSZ sphere, was analysed by three co-spaced electromagnetic detectors aligned coaxially with the pistol to measure flight time. The sabot velocity thus was detected at each sabot firing, based on the time-of-flight principle. The velocity of the sabot was assumed equal to that of the ejected sphere at short range.

2.3. Post-impact evaluation

After the impact test, surface damage to the SiC-particle/ and SiC-whisker/Si_3N_4 composites was investigated using optical microscopy and SEM, and their crater depths and diameters were measured by profilometory. Post-impact bending strength was measured by a four-point bending test (inner span 10 mm, outer span 30 mm) at a cross-head speed of 0.5 mm min^{-1}. The fractured surfaces were also examined using optical microscopy and SEM. The microstructures of these composites were examined using TEM.

3. Results and discussion

3.1. Mechanical properties and microstructre

The scanning electron micrographs in Figs 1a to d show the shapes of added SiC-whiskers and SiC-particles. The SiC-particles in Fig. 1a are very small having only a 0.3 μm diameter, and those in Fig. 1b are 30 to 100 μm diameter and under 10 μm thick. The latter are referred to as SiC-platelets. On the other hand, SiC-whiskers in Fig. 1c are straight and have diameters ranging from 0.5 to 1.0 μm, while the SiC-whiskers in Fig. 1d have a corrugated appearance and are 1 to 3 μm diameter.

Table II summarizes the mechanical properties of the hot-pressed SiC-particle/silicon nitride and SiC-whisker/silicon nitride composites containing the particles and whiskers listed in Table I. Compared to the matrix hot-pressed silicon nitride (HPSN(A)), the SiC-particle/Si_3N_4 (SiC-p/SN(B)) and SiC-whisker/Si_3N_4 (SiC-w/SN(D)) composites have lower densities, while the SiC-platelet/Si_3N_4 (SiC-pl/SN(C)) and large SiC-whisker/Si_3N_4 (L-SiC-w/SN(E)) composites have similar densities. All four composites, however, exhibit higher Young's moduli than the matrix, which is due to the effect of SiC addition and the dense microstructures produced by the hot-pressing process. SiC-p/SN(B) and SiC-w/SN(D) display higher hardness values than SiC-pl/SN(C) and L-SiC-w/SN(E) because the size of SiC additives used to make to SiC-p/SN(B) and SiC-w/SN(D) does not influence

TABLE I Properties of whiskers and particles

Properties		Si_3N_4 COA*	SiC-Particles		SiC-whiskers	
			Beta-SiC†	Platelet‡	1-0.7s§	SCW‡
Chemical composition (wt %)	N	> 38	–	–	–	–
	O	1.27	0.27	< 0.53	0.45	< 0.53
	C	< 0.3	0.40	–	0.20	–
	Al	< 0.05	0.04	–	0.29	–
	Ca	< 0.05	–	< 0.05	0.14	< 0.10
	Fe	< 0.1	0.05	< 0.005	0.04	< 0.005
	Mg	–	–	–	0.11	–
	Cr	–	–	< 0.011	–	< 0.011
Crystalographic structure		> 95 wt % Alpha-SN	Beta SiC	Alpha SiC	Beta SiC	Beta SiC
Diameter (μm)		0.5	0.26	20–70	0.78	1–3
Length (μm)		–	–	0.5–5 (thickness)	20–200	30–200
Specific density (g cm^{-3})		3.18	3.21	3.22	3.18	3.22
Surface area (m^2 g^{-1})		10.3	15.1	–	–	–

*Ube Industries Ltd. Akasaka, Tokyo, Japan.
†Ibiden Co. Ltd, Oogaki-city, Gifu-prefecture, Japan.
‡American Matrix Inc. 118 Sherlake Drive, Knoxville, Tennessee, USA.
§Tateho Chemical Industries, Akoh, Hyougo-prefecture, Japan.

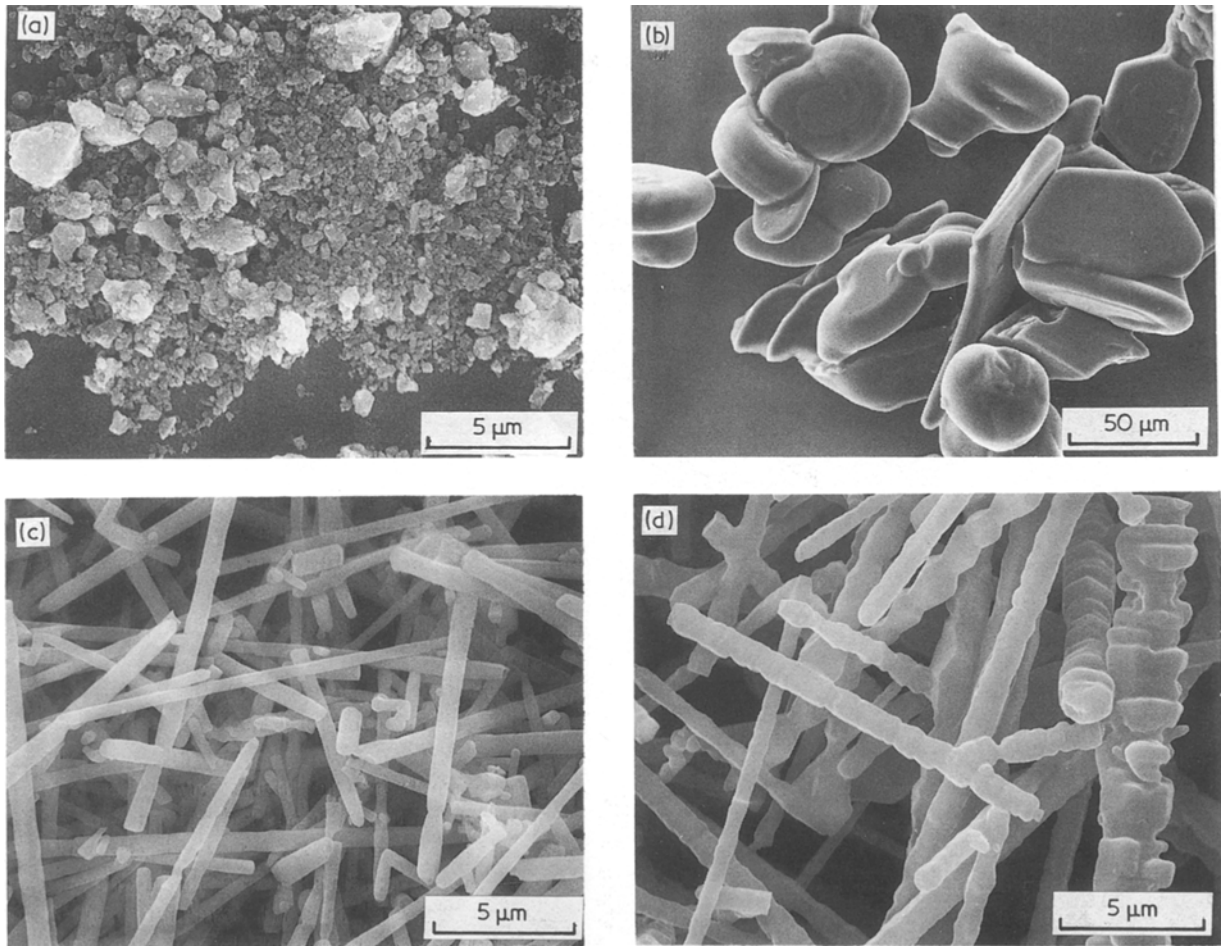

Figure 1 Scanning electron micrographs of SiC whiskers and particles used in this experiment. (a) SiC-particle (Ibiden, Japan); (b) SiC-platelet (American matrix, USA); (c) SiC-whisker (Tateho, Japan); (d) Large-SiC-whisker (American Matrix, USA).

matrix beta-Si_3N_4 grain development. On the other hand, SiC-pl/SN(C) and SiC-w/SN(E) display lower hardness values, which indicates that SiC addition influences their microstructures. This indicates that microscopic deformation behaviour of the composites when pressed by the Vickers indentor is influenced by their microstructures.

The addition of SiC-whiskers to the matrix effected a significant improvement in fracture toughness values (as seen in SiC-w/SN(D) and L-SiC-w/SN(E)), while the addition of SiC particles (as seen in SiC-p/SN(B) and SiC-pl/SN(C)) did not, at least within the range of this experiment. Figs 2a to e show the cross-sectional microstructures of the specimens broken in the bending test, HPSN(A) and SiC-p/SN(B) display similar microstructures in which small beta-Si_3N_4 grains are well distributed. However, the fracture surface is flat with large SiC platelets (arrow) in the case of SiC-pl/SN(C). Large SiC whiskers (arrow) are observed in the beta-Si_3N_4 matrix in the L-SiC-w/SN(E), and they create a complex fracture path. With SiC-w/SN(D) the SiC-whiskers cannot be distinguished well from the needle-like beta-Si_3N_4 grains. The SiC-whiskers in SiC-w/SN(D) and L-SiC-w/SN(E) strengthen the

TABLE II Mechanical properties of materials

Properties	HPSN	SiC-p/SN		SiC-w/SN		PSZ
	A	B†	C‡	D§	E‡	sphere
Relative density (% TD)	> 99	99	> 99	98	> 99	> 99
Crystal phase	beta-SN	beta-SN beta-SiC	beta-SN α-SIC	beta-SN beta-SiC	beta-SN beta-SiC	TZP
Bending strength (MPa)*	966	953	736	1032	978	1120
Weibull modulus	10.9	13	28	16.1	9.4	10
K_{IC}(MPa $m^{1/2}$)¶	5.7	5.4	5.7	6.0	6.8	7.5
Young's modulus (GPa)	284	295	295	295	295	200
Hardness, H_v (GPa)	18.9	20.2	15.8	18.8	16.0	12.5
H_v/H_p ratio	1.51	1.62	1.26	1.50	1.28	–
H/E ratio	0.067	0.068	0.054	0.064	0.054	–

*Four-point-bending test, ten specimens.
†, ‡, § see Table I.
¶ Indentation [26].

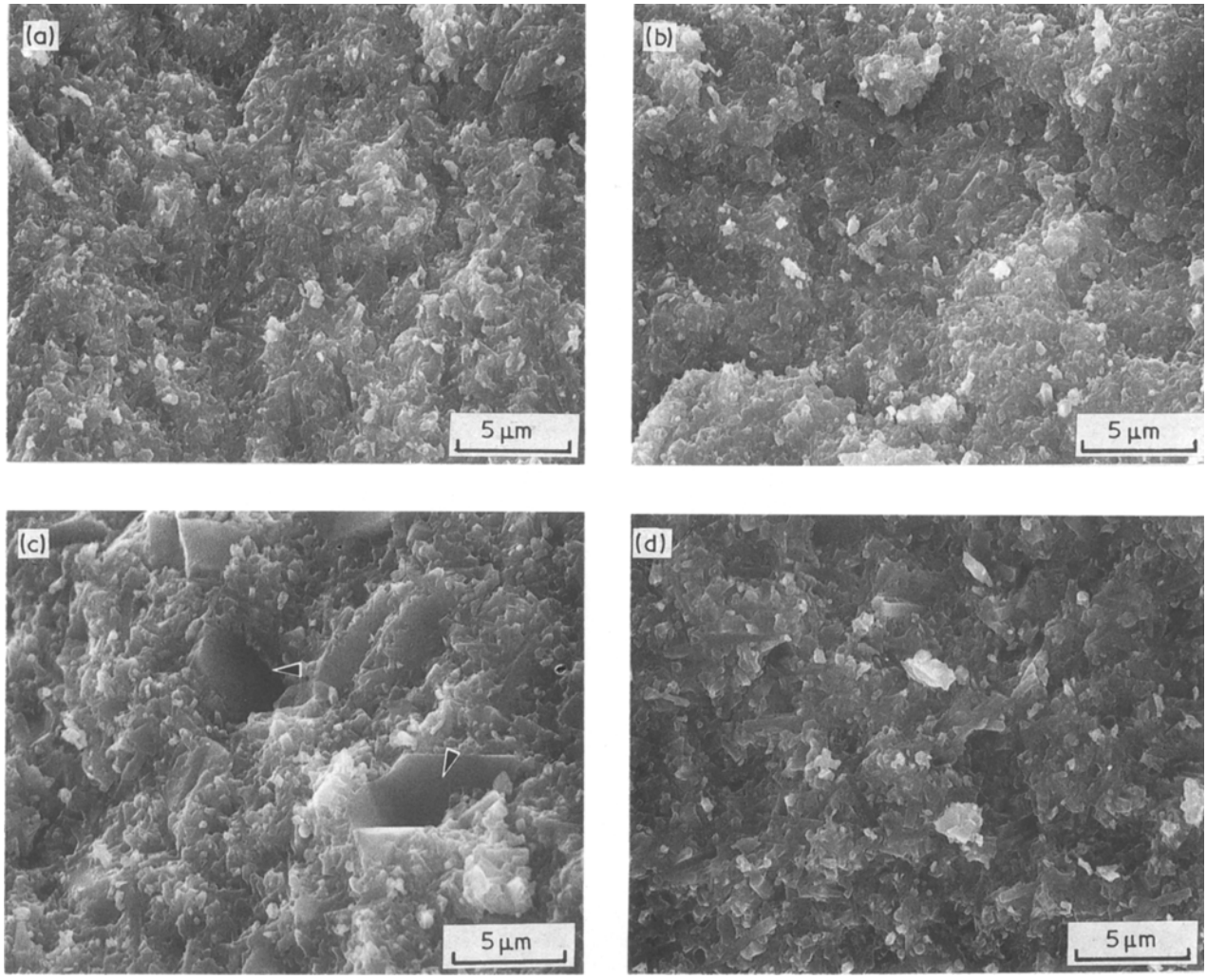

Figure 2 Scanning electron micrographs of fracture surface after bending test (arrow: SiC). (a) HPSN(A), (b) SiC-p/SN(B), (c) SiC-pl/SN(C), (d) SiC-w/SN(D), (e) L-SiC-w/SN(E).

composites' crack deflection mechanism giving them higher fracture toughness values than HPSN(A), SiC-p/SN(B), and SiC-pl/SN(C). No pull-out, however, was observed in any of the specimens.

Table II also provides bending-strength Weibull moduli for the matrix and the composites. Improvements in the Weibull modulus were made in the case of SiC-p/SN(B) and SiC-w/SN(D) with increasing bending strength while, with the exception of L-SiC-w/SN(E), bending strength level was maintained. Both the Weibull moduli and bending strengths of these composites are influenced by the microstructures formed through SiC addition. Large fracture origins were not observed in these composites, and the size of their fracture origins converged [7]. Only SiC-pl/SN(C) displayed a significant bending strength degradation due to fracture origin, which was the result of large SiC addition, even though it exhibited the highest Weibull modulus.

Figs 3a to e show the microstructures of these materials as observed using TEM. The silicon nitride matrix (in Fig. 3a) displays a microstructure in which elongated and small beta-Si_3N_4 grains are mixed, and these small grains can grow. The microstructure of SiC-p/SN(B) contains small SiC-particles mixed among small grains of beta-Si_3N_4 matrix, resulting in an under-developed microstructure. On the other hand, SiC-w/SN(D) and L-SiC-w/SN(E) exhibited somewhat deformed SiC-whiskers tightly packed together with Si_3N_4 grains in the microstructure [20]. Therefore, pullout does not occur in these composites at room temperature. Whisker deformation was caused by high pressure and heat during the hot-pressing process [27]. With SiC-pl/SN(C), only part of a large SiC piece is observed. Either this particle, which is probably a large SiC-particle, or its grain boundary is the origin of the fracture. Even though the same hot-pressing process was used, because the

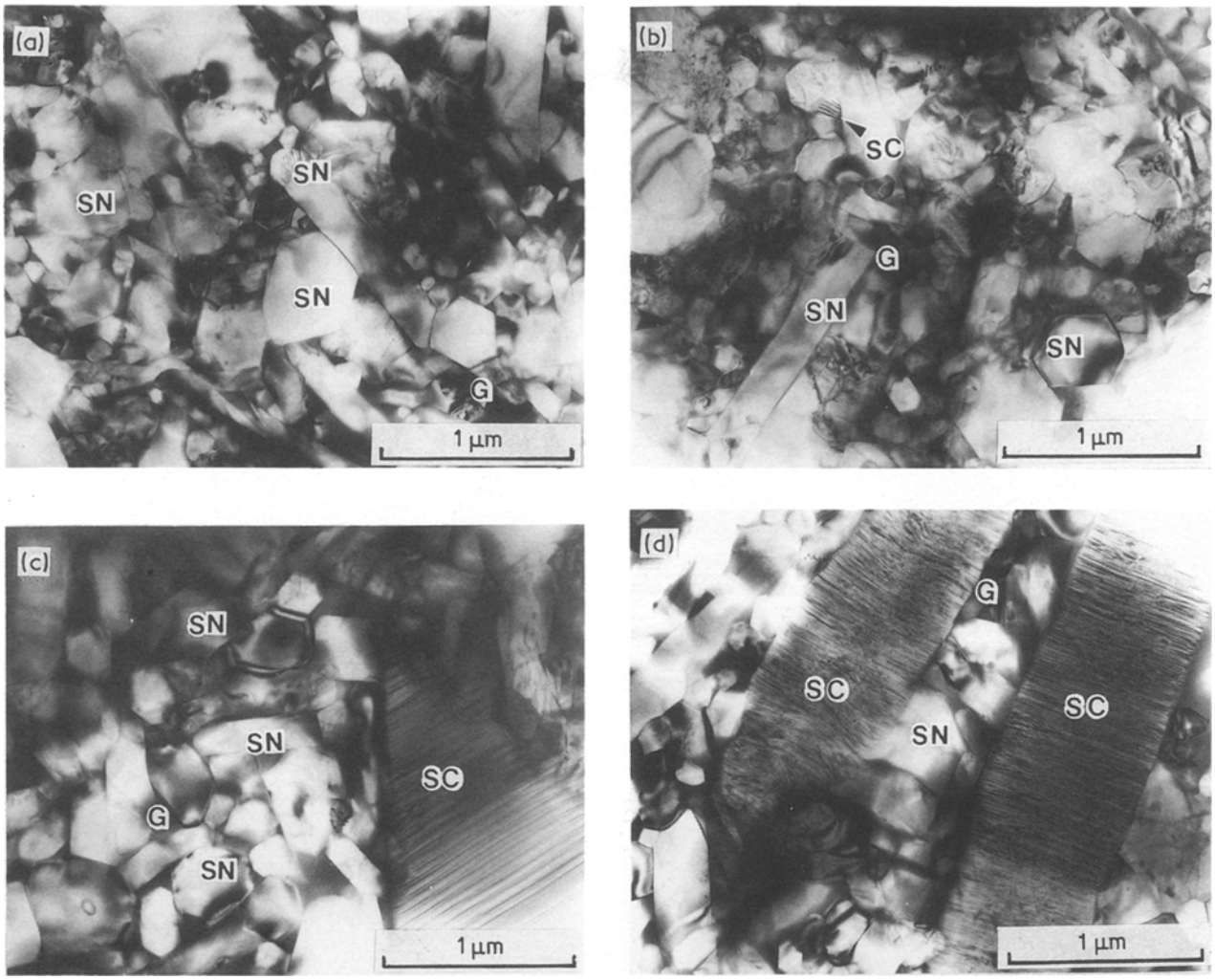

Figure 3 Transmission electron micrographs of five materials showing beta-Si_3N_4(SN), glassy layer(G), and SiC(SC). (a) HPSN(A), (b) SiC-p/SN(B), (c) SiC-pl/SN(C), (d) SiC-w/SN(D), (e) L-SiC-w/SN(E).

SiC-additives caused microstructural differences, the experimental conditions employed are not optimal for all the materials. Further research on the sintering process is required to obtain optimal conditions.

3.2. Post-impact evaluation

Figs 4a to e show surface damage to the matrix and the composites at impact volocities of 320 ± 10 m sec^{-1}. HPSN(A) is seen to have concentric ring cracks at the impact site, and SiC-p/SN(B) to have concentric ring cracks, radial cracks traversing the ring cracks, and lateral cracks. The other composites, however, only exhibit concentric ring cracks and small radial cracks at the impact site. Judging from these surface-damage observations alone, HPSN(A), which has only ring cracks, displays elastic response behaviour, and SiC-p/SN(B), SiC-pl/SN(C), SiC-w/SN(D), and L-SiC-w/SN(E), which have radial and lateral cracks, display elastic/plastic response behaviour. The latter three composites (C, D, and E) display a higher degree of elastic response than SiC-p/SN(B). Because response behaviour cannot be determined through surface observations alone, the fractured surfaces were examined.

Figs 5 and 6, in which crater depth and diameter are measured using a profilometer, show that there is no significant difference in the crater sizes of the five materials. Crater diameter and depth may be related to the hardness value; however, this was not reflected in the results. With dynamic impact, sphere penetration, sphere fragmentation and target deformation behaviour combine to create to crater geometry which measures about the same size when using a profilometer. Crater depth increases rapidly when the impact velocity exceeds 300 m sec^{-1}, and deformation behaviour changes at around this velocity without affecting crater diameter. The deformation process of structural compaction, microcracking, and Hertz cone-cracking also become significant at around this velocity. As a result, crater geometry does not

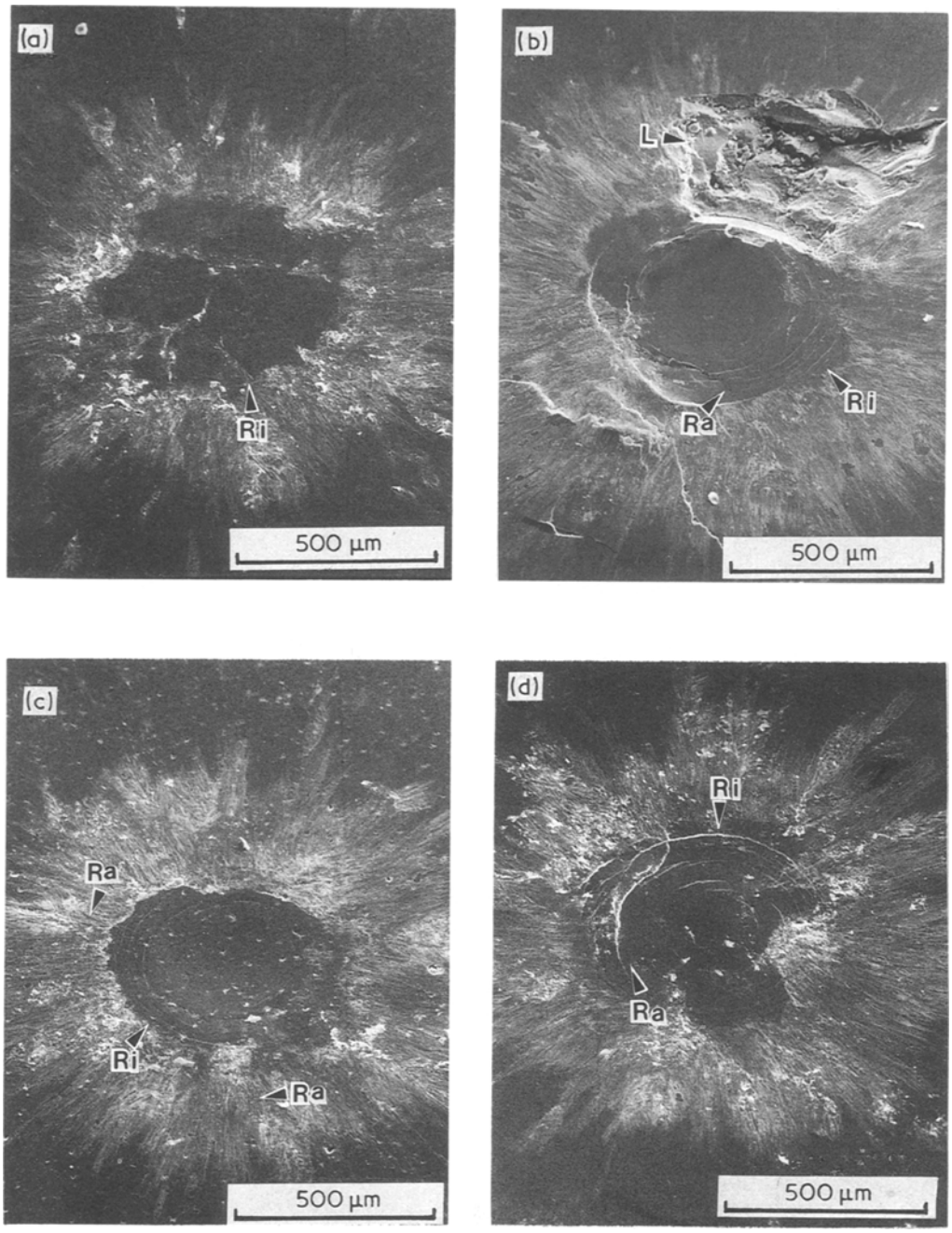

Figure 4 Surface damage morphologies for five materials showing, Ring crack (Ri), Radial crack (Ra), and Lateral crack (L) ($V = 320 \pm 10\,\mathrm{m\,sec^{-1}}$). (a) HPSN(A), (b) SiC-p/SN(B), (c) SiC-pl/SN(C), (d) SiC-w/SN(D), (e) L-SiC-w/SN(E).

completely reflect the results of statically-measured hardness.

Fig. 7 illustrates the residual bending strength of these impacted specimens. Except for SiC-pl/SN(C), a two-step strength degradation process occurs. The first step (30% to 50% degradation) takes place at a low impact velocity range, and the second (50% to 80% degradation) occurs at a high impact velocity range. Only SiC-pl/SN(C) exhibits a one-step strength degradation process, as supported in the literature [20, 23]. Impact-induced subsurface cracks just under the impact site are larger than the inherent flaw size in the first strength degradation step, and they gradually enlarge until the second degradation step when they grow into large cracks. The fractured surfaces of the

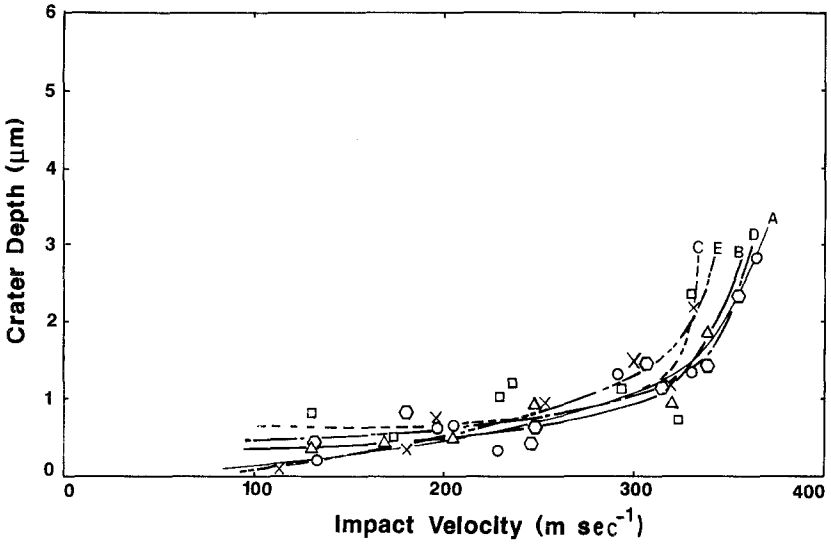

Figure 5 Crater depths. (—○—) HPSN(A), (—△—) SiC-p/SN(B), (- - -□- - -) SiC-pl/SN(C), (-—◇—-) SiC-w/SN(D), (- - -x- - -) L-SiC-w/SN(E).

specimens were examined to analyse the damage phenomena.

Figs 8a to i show the surfaces of cross-sectional fracture and the crack was initiated on the surface. Even in the first degradation step, except for SiC-pl/SN(C) cone cracks are initiated just under the impact site. Figs 8a, c, f and h show small cone-crack initiation in HPSN(A), SiC-p/SN(B), SiC-w/SN(D), and L-SiC-w/SN(E) even at first step impact velocity, indicating that cone-crack initiation occurs more readily in these composites. Large Hertz cone-cracks (in Figs 10b, d, e, g and i) were initiated in HPSN(A), SiC-p/SN(B), SiC-pl/SN(C), SiC-w/SN(D), and L-SiC-w/SN(E) when impact velocity exceeded their critical values (V_c). Strength degradation occurred when impact velocity reached 300 m sec^{-1}. This result implies that Hertz cone cracks are initiated as the result of stress produced at impact; they then extend down to the subsurface region upon successive loading. A critical stress level is believed to be required to initiate a cone crack and a critical energy level to extend it [15, 22]. Added SiC to the beta-Si_3N_4 matrix influences the Hertz cone-crack formation and propagation process [20]. A detailed analysis of the mechanisms behind cone-crack initiation and propagation will be conducted as the topic of future research.

The microstructural changes produced by SiC addition are to exert an influence on Hertz cone-crack initiation and crack propagation. In comparison to HPSN(A), SiC-w/SN(D) and L-SiC-w/SN(E) display better crack propagation resistance, and SiC-pl/SN(C) displays better crack initiation resistance. On the other hand, SiC-p/SN(B) did not exhibit resistance to Hertz cone-crack damage. With SiC-p/SN(B), significant cone cracks were observed on the fracture surface at a low-to-medium impact velocity range. The results showed that the shape of the SiC additives and the mechanical properties of the composites including hardness and fracture toughness, have an influence on crack initiation and propagation.

Composite microstructures differ according to the shape of the SiC additives [11]. Similarly, mechanical properties differ according to the microstructure of silicon nitride after SiC addition [11]. Not only the mechanical properties, but also the impact damage behaviour were different for each composite in this experiment. The relationship between hardness, which determines the deformation behaviour of the microstructure, and damage behaviour was explored.

Hardness is defined as an elastic/plastic parameter in the literature [28]. The ratio of target material hardness to particle hardness (H_t/H_p) is determinant of target response behaviour. Schockey *et al.* [16] showed that target response behaviour is affected by changes

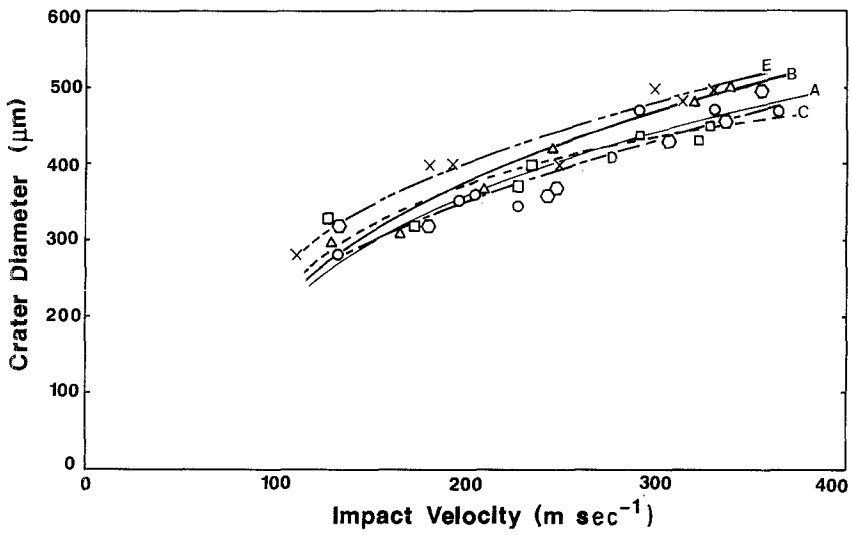

Figure 6 Crater diameters. For key, see Fig. 5.

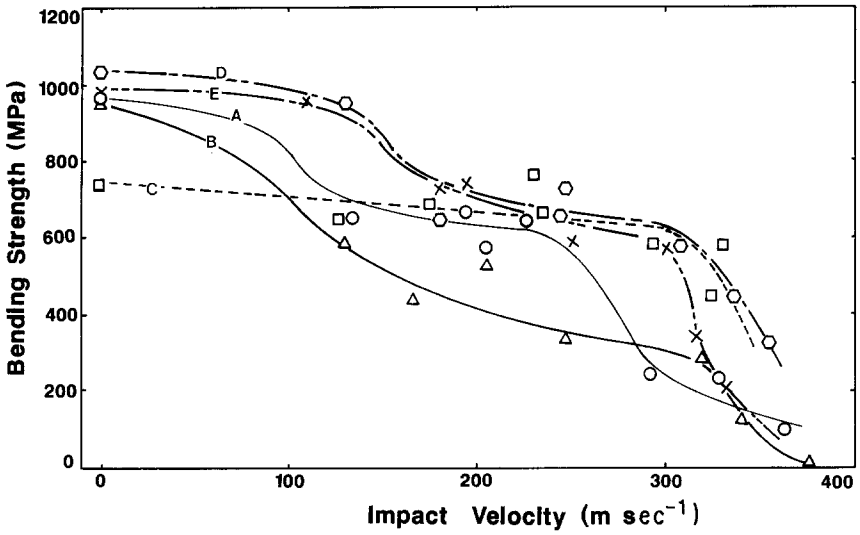

Figure 7 Residual bending strength of impacted specimens showing two types of strength dedgradations. For key, see Fig 5.

in the H_t/H_p ratio. The H_t/H_p ratios used in this experiment are summarized in Table II, and their values as well as those of Young's modulus and hardness are within the elastic response region [24]. The addition of smaller particles yields composites with larger H_t/H_p ratios, which display higher elastic responses than the composites made with large SiC additives. Craters observed on the surface of all the specimens showed them to have elastic/plastic response behaviour; however, Hertz cone cracks revealed through the bending test showed their dominant response behaviour to be elastic.

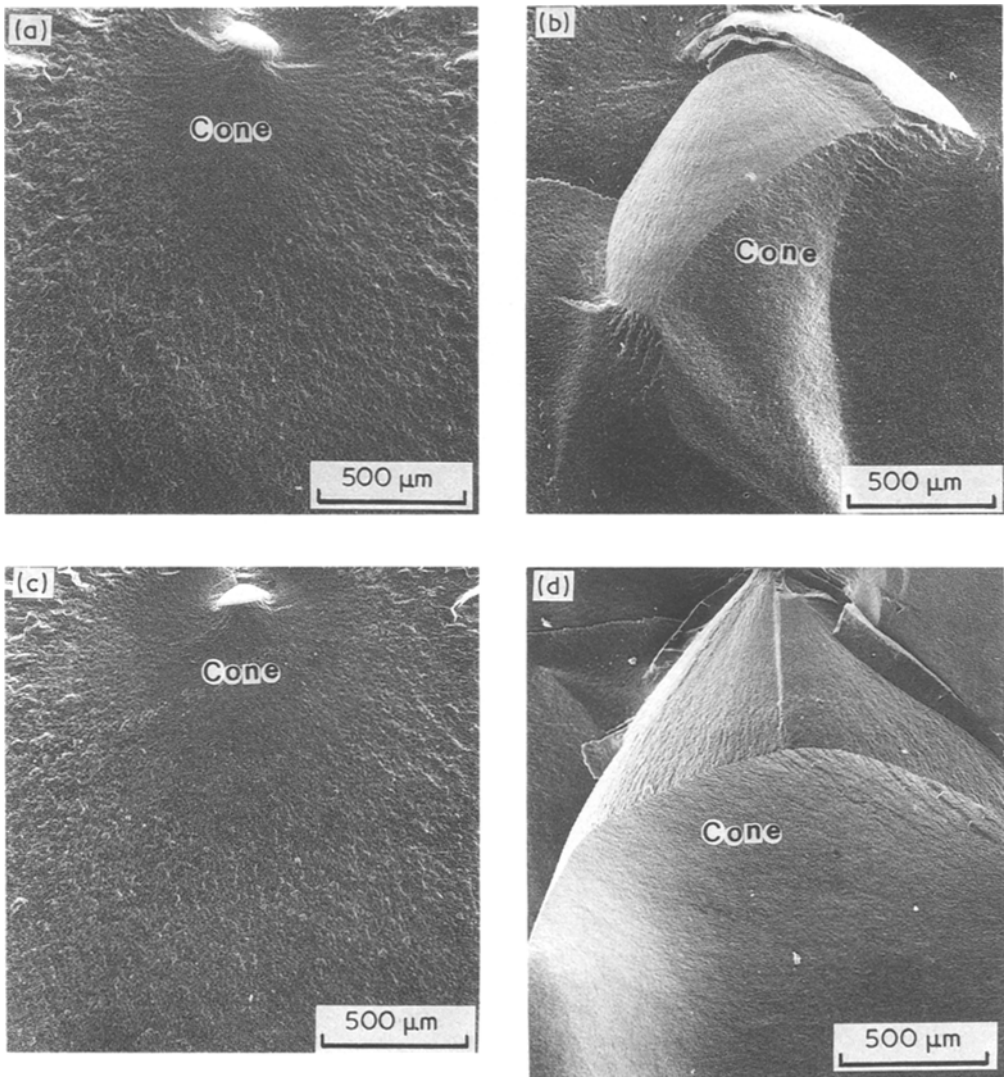

Figure 8 Scanning electron micrographs of fracture surfaces showing Hertz cone-crack initiation. (a) HPSN(A) at $V = 205\,\mathrm{m\,sec^{-1}}$, (b) HPSN(A) at $V = 330\,\mathrm{m\,sec^{-1}}$, (c) SiC-p/SN(B) at $V = 205\,\mathrm{m\ sec^{-1}}$, (d) SiC-p/SN(B) at $V = 329\,\mathrm{m\,sec^{-1}}$, (e) SiC-pl/SN(C) at $V = 321\,\mathrm{m\,sec^{-1}}$, (f) SiC-w/SN(D) at $V = 246\,\mathrm{m\,sec^{-1}}$, (g) SiC-w/SN(D) at $V = 335\,\mathrm{m\,sec-1}$, (h) L-SiC-w/SN(E) at $V = 249\,\mathrm{m\ sec^{-1}}$, (i) L-SiC-w/SN(E) at $V = 330\,\mathrm{m\,sec^{-1}}$.

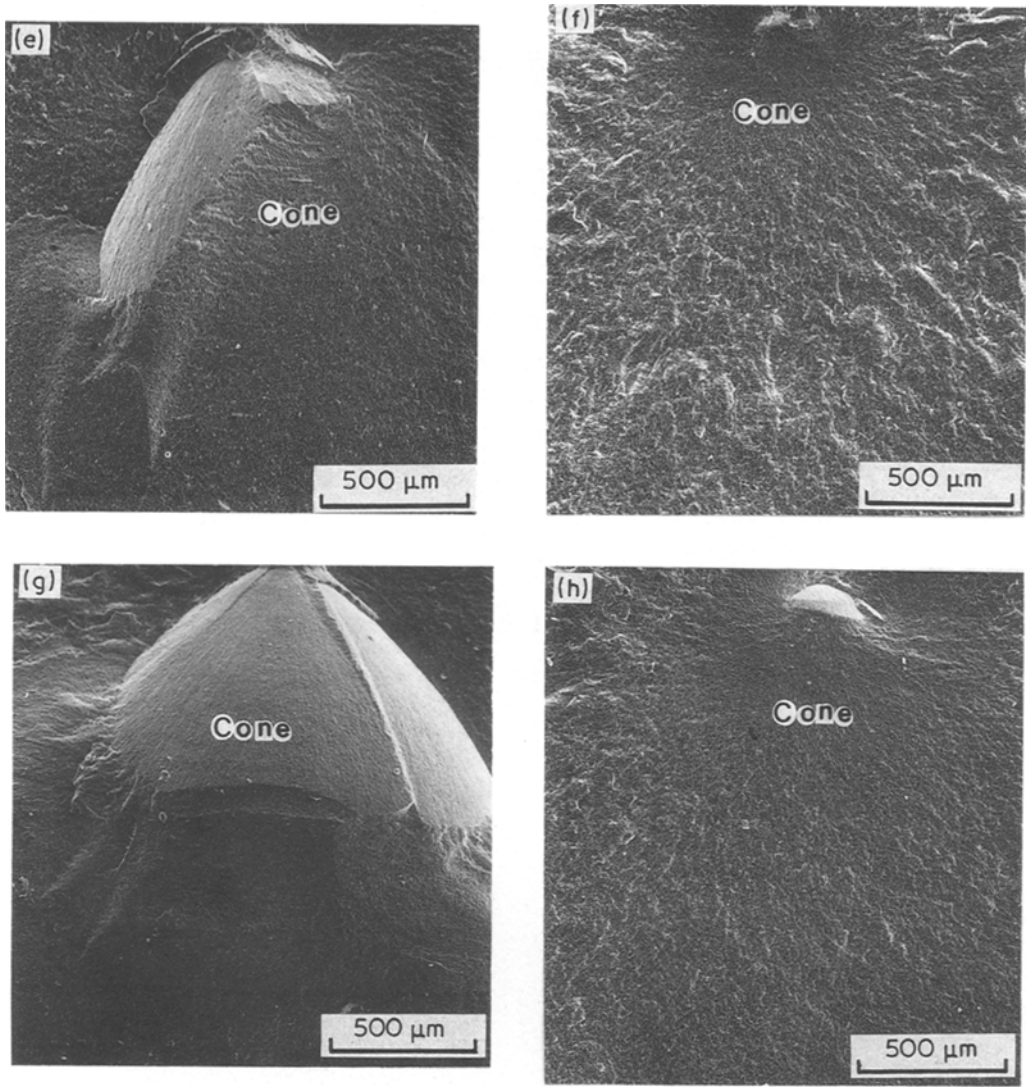

Figure 8 Continued.

Lawn and Howes [28] defined the response behaviour of ceramic materials using the Vickers indentation method. When a spherical indentor is used, elastic recovery of the crater diameter occurs after sphere deformation and fragmentation, which makes it impossible to determine the ratio of crater diameter to depth. However, the hardness to Young's modulus (H/E) ratio of the target material is defined as an elastic/plastic parameter [28], and H/E values are related to Hertz cone-cracking initiation. SiC-p/SN(B) and SiC-w/SN(D) have higher H/E ratios (0.064 to 0.068) than SiC-pl/SN(C) and L-SiC-w/SN(E) (0.054), which indicates that larger particles and whiskers yield lower hardness and, as a result, a higher degree of elastic/plastic response behaviour even though their dominant response behaviour is elastic. Larger platelets and whiskers affected the sintering behaviour of silicon nitride powder, resulting in greater microstructure deformability. The addition of larger particles yields composites that incur larger deformation under point impact. The lower hardness values of these composites enable better impact energy dissipation. Therefore, SiC-pl/SN(C) achieved a higher degree of resistance to impact.

4. Conclusion

SiC-whisker/Si_3N_4 and SiC particle/Si_3N_4 composites were produced by hot-pressing and the relationship between their mechanical properties and impact damage was examined. Both the matrix HPSN(A) and all of the composites showed elastic response behaviour, with Hertz cone crack initiation. SiC-whisker/SN(D) showed the highest bending strength among the specimens, but had less impact resistance, while L-SiC-w/SN(E) showed the highest fracture toughness with moderate impact damage resistance. SiC-p/

SN(B) showed the highest hardness, but the least impact damage resistance, while SiC-platelet/SN(C) showed the highest impact damage resistance, but the lowest Vickers hardness and bending strength. With SiC-pl/SN(C), the addition of larger particles caused a decrease in composite hardness without pore introduction. This enabled better impact energy dissipation, which means higher impact resistance.

Acknowledgements

I would like to extend my sincere appreciation to Mr M. Mukai and Mr H. Matsuura for their assistance with the experiments.

References

1. W. RICHERSON, *Amer. Ceram. Soc. Bull.* **64** (1985) 282.
2. G. L. BOYD and D. M. KREINER, in the Proceedings of the 25th Automotive Technical Development Contractor's Coordination Meeting, P-209, (Society of Automobile Engineer, Pennsylvania, (1988) pp. 101-23.
3. D. K. HALE and A. KELLY, *Ann. Rev. Mater. Sci.* **2** (1972) 405.
4. K. T. FABER and A. G. EVANS, *Acta Metall* **31** (1983) 565.
5. D. J. GREEN, *Commun. Amer. Ceram. Soc.* **66** (1983) c4.
6. R. W. RICE, *Ceram. Engng. Sci. Proc.* **2** (1981) 661.
7. K. UENO and Y. TOIBANA, *Yogyo-Kyokaishi* **91** (1983) 491.
8. P. D. SHALEK, J. J. PETROVIC, G. F. HURLEY and F. D. GAC, *Amer. Ceram. Soc. Bull.*. **65** (1986) 351.
9. S. T. BULJAN, J. G. BALDONI and M. L. HUCKABEE, *ibid.* **66** (1987) 347.
10. P. GEIL, G. PETZOW and H. TANAKA, *Ceram. Int.* **13** (1987) 19.
11. H. YEH, H. FANG and K. TEMG, *Ceram. Engng. Sci. Proc.* **9** (1988) 1333.
12. G. WOTTING and G. ZIEGLER, *Ceram. Int.* **10** (1984) 18.
13. P. F. BECHER, C. H. HSUEH, P. ANGELINI and T. N. TIEGS, *J. Amer. Cram. Soc.* **71** (1988) 1050.
14. Z. LI and R. C. BRADT, *J. Amer. Ceram. Soc.* **72** (1989) 70.
15. K. C. DAO, D. A. SHOCKEY, L. SEAMON, D. R. CURRAN and D. J. ROWCLIFFE, Annual Reports, Part III, Office of Naval Research, Contract No. N00014-76-057, May 1979.
16. D. A. SHOCKEY, D. C. ERLICH and K. C. DAO, *J. Mater. Sci.* **16** (1981) 477.
17. J. CUSSIO and H. FANG, in the Proceedings of the 26th Automotive Technology Development, Coordination Meeting (Society of Automobile Engineer, Pennsylvania, (1988) p. 281.
18. C. T. MORRISON, J. L. ROUTBORT and R. O. SCATTERGOOD, *Mater. Res. Soc. Symp. Proc.* **78** (1987) 207.
19. R. A. PAGE, C. R. BLANCHARD-ARDID and W. WEI, *J. Mater. Sci.* **23** (1988) 946.
20. Y. AKIMUNE, Y. KATANO, K. MATOBA, *J. Amer. Ceram. Soc.* **72** (1989) 791.
21. H. R. HERTZ, "Hertz's Miscellaneous Papers", (McMillan, London 1896) Chs 5 and 6.
22. B. R. LAWN and T. R. WILSHAW, *J. Mater. Sci.* **10** (1975) 1049.
23. S. M. WIEDERHORN and B. R. LAWN, *J. Amer. Ceram. Soc.* **60** (1977) 451.
24. Y. AKIMUNE, Y. KATANO and K. MATOBA, in the Proceedings of the 3rd Symposium for Ceramic Materials and Components for Engines V. J. Tenney (ed.) p. 1495 (American Ceramic Society).
25. W. WEIBULL, *J. Appl. Mech.* **18** (1951) 293.
26. B. R. LAWN and E. R. FULLER, *J. Mater. Sci.* **10** (1975) 2016.
27. V. K. SARIN and M. RUHLE, *Composite* **18** (1987) 129.
28. B. R. LAWN and V. R. HOWES, *J. Mater. Sci.* **16** (1981) 2745.

Received 10 April
and accepted 28 September 1989